Vulnerability in dynamically driven oscillatory networks and power grids

Cite as: Chaos **30**, 063111 (2020); doi: 10.1063/1.5122963
Submitted: 4 August 2019 · Accepted: 12 May 2020 ·
Published Online: 1 June 2020 · Corrected: 12 June 2020

Xiaozhu Zhang,[1,a)] Cheng Ma,[2] and Marc Timme[1,a)]

AFFILIATIONS

[1]Chair for Network Dynamics, Institute for Theoretical Physics and Center for Advancing Electronics Dresden (cfaed), Cluster of Excellence Physics of Life, Technical University of Dresden, 01062 Dresden, Germany
[2]School of Physics, Nankai University, Tianjin 300071, China

Note: This paper is part of the Focus Issue on the Dynamics of Modern Power Grids.
[a)]**Authors to whom correspondence should be addressed:** xiaozhu.zhang@tu-dresden.de and marc.timme@tu-dresden.de

ABSTRACT

Vulnerability of networks has so far been quantified mainly for structural properties. In driven systems, however, vulnerability intrinsically relies on the collective response dynamics. As shown recently, dynamic response patterns emerging in driven oscillator networks and AC power grid models are highly heterogeneous and nontrivial, depending jointly on the driving frequency, the interaction topology of the network, and the node or nodes driven. Identifying which nodes are most susceptible to dynamic driving and may thus make the system as a whole vulnerable to external input signals, however, remains a challenge. Here, we propose an easy-to-compute Dynamic Vulnerability Index (DVI) for identifying those nodes that exhibit largest amplitude responses to dynamic driving signals with given power spectra and thus are most vulnerable. The DVI is based on linear response theory, as such generic, and enables robust predictions. It thus shows potential for a wide range of applications across dynamically driven networks, for instance, for identifying the vulnerable nodes in power grids driven by fluctuating inputs from renewable energy sources and fluctuating power output to consumers.

Signal-induced large excursions of the dynamics of networked systems may pose risks to system functionality. For instance, in power grids, large frequency excursions from the nominal value (of 50 Hz or 60 Hz) become more frequent with a larger share of renewable energy sources, posing serious challenges for grid operation and control. Because external signals are often stochastic and a network's response pattern is dynamic, highly heterogeneous, and depends on the network structure and the frequency statistics of the input signal, it remains an open problem to determine which nodes are most vulnerable to fluctuating network inputs. Here, we propose a Dynamic Vulnerability Index (DVI) to identify those nodes with largest frequency responses to stochastic power fluctuations that drive a network at any unit. The index takes into account the distributed and time-dependent nature of the network responses and is computable in a straightforward and fast way.

I. INTRODUCTION

Oscillatory networks, modeling the underlying mechanisms of many real-world systems ranging from gene and neural circuits[1,2] to AC power grids,[3–8] exhibit highly nontrivial responses to external driving signals,[9–13] due to the complexity in the underlying topology and the nonlinearity in the coupling function. Recently, growing attention has been drawn to the topic of dynamically driven networks in part because of the important application of the second-order Kuramoto-type oscillator model in power grid operation and control.[12–16] With an increasing share of fluctuating renewable energy sources integrated in modern power grids, it is crucial for grid operators to predict the distributed frequency responses to systematic and stochastic fluctuations and to identify which units are most susceptible and may thus make the system as a whole vulnerable to dynamic inputs.

For the example of power grid models, key aspects of network responses to dynamical perturbations have been uncovered recently: about the impact of various types of perturbation signals, including the scaling in the relaxation of power grids after pulse-like perturbations,[15,16] the differential response to static perturbations,[17] the distributed dynamic patterns in response to dynamic perturbations,[12] the fluctuation-induced non-Gaussian grid frequency distribution,[18] and the escape of a system from an operation state if driven by white noise[14] and/or non-Gaussian noises.[19,20] Specifically, the time-averaged nodal deviations from the network mean response were ranked using a centrality measure based on the Laplacian spectrum.[21] For lossy networks, averaged nodal sensitivity to fluctuations across networks have been numerically investigated[22] and estimated via the nodal variance.[23] Yet, it is still unclear which stochastic signals may cause network-wide response patterns and how to quickly and precisely identify those nodes that potentially exhibit most severe responses and thus are most vulnerable to such perturbations.

The core of the puzzle lies in an intriguing phenomena of dynamic network resonance,[12] which is present in oscillator models with two (or more) variables per node (such as the second-order Kuramoto model, an oscillatory power grid model) but not in the networks of phase oscillators such as in the original Kuramoto model.[9–12] While the network responses for low- and high-frequency signals are trivial thus fairly predictable—homogeneous responses for slowly changing signals and localized responses for fast-changing signals—fluctuations in the resonance frequency regime of a network system induce complex resonance patterns in oscillatory networks.[12] The patterns are jointly determined by the perturbation frequency, the underlying network topology, the initial unperturbed network state (base operating state), and the location of the perturbation and the response of interest. Although the resonant responses can be deterministically and precisely computed for given perturbation time series deriving and evaluating a linear response theory,[12] a straightforward, fast, and reliable method for estimating the resonant response strengths for stochastic signals is still missing mainly because such signals contain an extended band of frequencies.

Here, going beyond structural vulnerability in networks, we propose the Dynamic Vulnerability Index (DVI), a computationally inexpensive vulnerability measure to assess and to rank the largest possible resonant response of individual nodes in oscillatory networks. The networks are driven by stochastic perturbations containing a characteristic power spectral density (PSD) function. In power grid research and beyond, the term *network vulnerability* is typically used to describe the impact of purely topological changes on network performance.[24–28] The meaning of the *vulnerability* of a node was extended to considering the node's transient response to a pulse-like perturbation[29,30] and recently to the time-averaged response to stochastic perturbations.[21] Here, we propose a Dynamic Vulnerability Index (DVI) that expands the definition by considering the global maximum of a node's *dynamic* response to a *stochastic* input signal. Employing a linear response theory[12] and a frequency-specific estimate of the resonant response strength, the DVI exhibits high prediction power and helps in identifying those nodes potentially respond most strongly to a stochastic resonant perturbation and thereby posing systemic risks in power grid stability. Specifically, the DVI identifies the vulnerable nodes at unexpected locations in the network not foreseeable from the topology alone.

II. RESONANT NETWORK RESPONSE PATTERNS

Consider a network of N second-order Kuramoto-type oscillators with dynamics governed by

$$\ddot{\theta}_i = P_i - \alpha\dot{\theta}_i + \sum_{j=1}^{N} K_{ij}\sin(\theta_j - \theta_i) + \delta_{ik}D(t) \tag{1}$$

and driven by an external fluctuating signal $\delta_{ik}D(t)$ only present at node k. Here, θ_i and P_i denote the rotation angle and the natural acceleration of the oscillator i (proportional to the power input or output at i), $\alpha > 0$ parametrizes the damping coefficient, and $K_{ij} > 0$ denotes the coupling strength of the node pair (i,j). The model is equivalent to a coarse-grained model of AC power grids[12] enabling effective inertia for sub-grids, where sub-grids are modeled as oscillatory nodes with fluctuating power inputs from renewable sources. It describes the collective dynamics of N sub-grids at a set grid frequency of $\Omega_0 = 2\pi \times 50\,\mathrm{Hz}$ (or 60 Hz in the USA and parts of Japan) in the normal operation state. The effective damping coefficient α characterizes the effective windage losses during the rotation of the generators and turbines in the sub-grids. In this context, θ_i represents the center-of-inertia angle deviation of the sub-grid i to the reference frame rotating at Ω_0; thus, $\dot{\theta}_i$ represents the deviation of the grid frequency at the sub-grid i to its nominal value Ω_0. P_i is related to the power generated ($P_+ > 0$) or consumed ($P_- < 0$) in the sub-grid i and K_{ij} the line capacity of the power transmission between the sub-grid i and j. The driving signal $\delta_{ik}D(t)$ is a fluctuating time series additive to the average power generation or consumption at the sub-grid k. For the purpose of the modeling setup, each sub-grid is presented as one node of a graph.

How does such a network respond to dynamic input signals (Fig. 1)? Close to a normal operation state of the power grid, i.e., a stable fixed point $\boldsymbol{\theta}^* := (\theta_1^*, \ldots, \theta_N^*)$ of the oscillatory network, the collective response $\boldsymbol{\Theta}(t) := \boldsymbol{\theta}(t) - \boldsymbol{\theta}^*$ to a perturbation vector $\mathbf{D}^{(k)}(t)$ defined via its components $D_i^{(k)}(t) := \delta_{ik}D(t)$ is accurately given by a linear response theory,[12]

$$\ddot{\boldsymbol{\Theta}}^{(k)} = -\alpha\dot{\boldsymbol{\Theta}}^{(k)} - \mathcal{L}\boldsymbol{\Theta}^{(k)} + \mathbf{D}^{(k)}, \tag{2}$$

where $\mathcal{L}$ with $\mathcal{L}_{ij} := K_{ij}\cos(\theta_j^* - \theta_i^*)$ for $i \neq j$ and $\mathcal{L}_{ii} = -\sum_{j\neq i}\mathcal{L}_{ij}$ is a weighted graph Laplacian. The linear network response is analytically solvable by projecting it to the orthogonal eigenspaces of the Laplacian matrix.[12] For a perturbation $D(t) = \varepsilon(\omega)e^{\imath[\omega t + \varphi(\omega)]}$ at the unit k of a given frequency, the *frequency response* $\dot{\Theta}_i^{(k)}$ at the unit i, i.e., the response in unit i's angular velocity $\dot{\theta}_i$, approaches an invariant (steady) state

$$\dot{\Theta}_i^{(k)}(\omega, t) = \varepsilon(\omega)e^{\imath[\omega t + \varphi(\omega)]}\sum_{\ell=0}^{N-1}\frac{\imath\omega\nu_k^{[\ell]}\nu_i^{[\ell]}}{-\omega^2 + \imath\alpha\omega + \lambda^{[\ell]}} \tag{3}$$

as $t \to \infty$ with the same frequency ω as the driving signal but with a node-specific magnitude and a phase shift. In the context of power grid dynamics, Eq. (3) gives the steady-state response in the electric AC frequency at the node (sub-grid) i. Here, $\lambda^{[\ell]}$ and

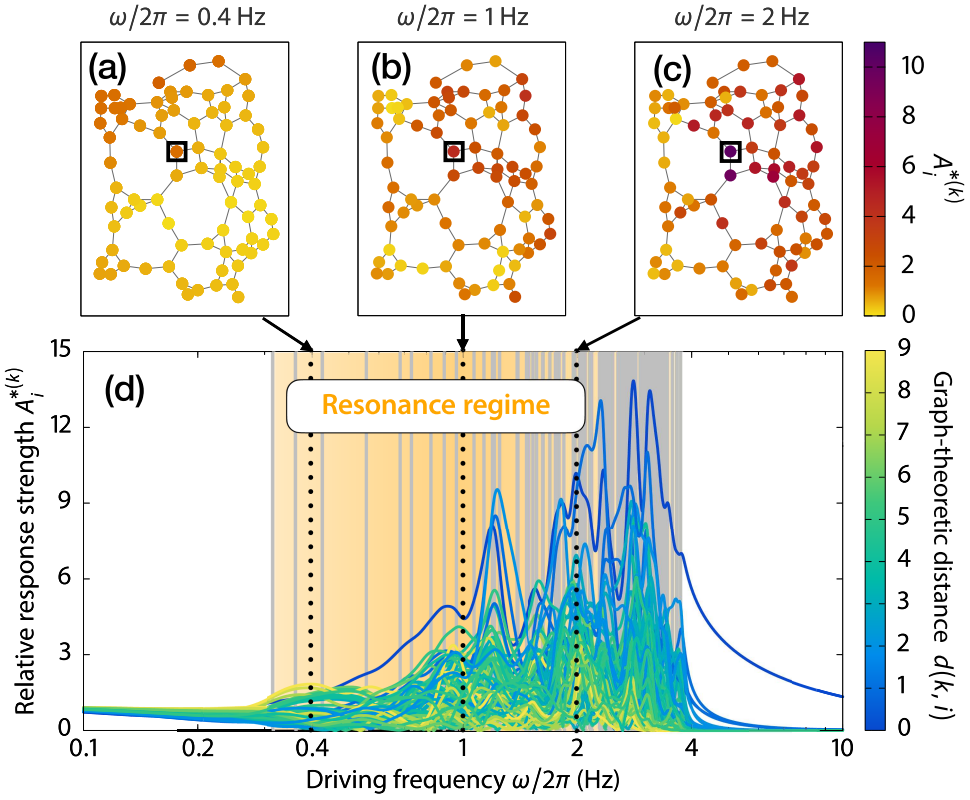

FIG. 1. Complex network resonance patterns and large amplitude responses. (a)–(c) Distinct network resonance patterns for three driving frequencies. Each node is color-coded by the relative response strength $A_i^{*(k)} := |\dot{\Theta}_i^{(k)}|/\lim_{\omega\to 0}|\dot{\Theta}_i^{(k)}|$, and the driven node is marked with a black square. In simulation, we use per-unit parameters $\alpha = \Omega_0\bar{D}/2\bar{H}$, $P_+ = \Omega_0/2\bar{H}$, $P_- = -P_+/3$, and $K_{ij} = 2P_+$ with the normalized damping coefficient $\bar{D} = 0.02\,\mathrm{s}^2$ and the aggregated inertia constant $\bar{H} = 4\,\mathrm{s}$. The network topology is created by a random growth model of power grid networks.[31] (d) The resonant response patterns varies with the driving frequency in the resonance regime (shaded orange). The relative response strength of an individual node i is color-coded by its *graph-theoretic distance* $d(k,i)$ (also abbreviated as "distance" in this work) to the driven node k, which is defined as the number of edges in a shortest path between a node pair. Gray vertical lines indicate the $N-1$ resonance frequencies $\omega_{\mathrm{res}}^{[\ell]}$.

$v_i^{[\ell]}$ denote, respectively, the ℓth eigenvalue and the ith component of the corresponding eigenvector. The eigenvalues are indexed as $0 = \lambda^{[0]} \le \cdots \le \lambda^{[N-1]}$. When one of the eigenmodes is excited, that is, when the perturbation frequency ω maximizes the contribution of an eigenmode in Eq. (3) with an eigenfrequency,

$$\omega = \omega_{\mathrm{res}}^{[\ell]} := \sqrt{\lambda^{[\ell]} - \frac{\alpha^2}{4}}, \tag{4}$$

the network response is dominated by the resonant eigenmode characterized by an overlap factor $v_k^{[\ell]}v_i^{[\ell]}$, constituting a nontrivial, highly heterogeneous dynamic pattern (Fig. 1).

We emphasize that network resonances emerge not only at a single perturbation frequency, but at all $N-1$ frequencies in a wide frequency range,

$$\omega \in I_{\mathrm{res}} := \left[\sqrt{\lambda^{[1]} - \frac{\alpha^2}{4}}, \sqrt{\lambda^{[N-1]} - \frac{\alpha^2}{4}}\right]. \tag{5}$$

This interval marks the *resonance regime*, with responses substantially increased due to resonances still extending to outside the interval. Extraordinarily high strengths of the frequency response up to an order-of-magnitude (e.g., 12 times) larger than the homogeneous response strength in the low frequency limit[12] may appear across the network [Fig. 1(d)]. Furthermore, the resonant response pattern sharply depends on the driving frequency. In an exemplary network, the response pattern appears to be distinctly different for three frequencies with no more than 1 Hz apart from each other [Figs. 1(a) and 1(c)]. Besides the heterogeneity in response amplitudes, each node's response additionally exhibits a heterogeneous phase delay toward the perturbation signal due to the characteristic arguments of the complex responses (3).

III. INDEXING RESONANT RESPONSES

Even perturbed only by a single-frequency resonant signal, the network already exhibits complex response patterns in terms of the strength and the phase delay of the sinusoidal response (3). In reality, power grids are constantly exposed to noisy fluctuations in renewable power generation and in the power consumption of households and industry, which consist of Fourier components with a wide range of frequencies in the resonance regime, stochastic magnitudes, and random phases. For a given noisy perturbation time series, the network response time series is computable by summing up the linear response to each frequency (3). However, the influence of future remains unknown. Making general predictions for a network's complex resonant response to noisy fluctuations and, particularly, identifying the most susceptible nodes still remains a challenge.

We propose an index of the vulnerability of individual nodes in a network under resonant perturbations, the Dynamic Vulnerability Index (DVI), which helps in ranking the maximum resonant response magnitude for perturbations with a characteristic PSD $S(\omega)$. Measurements of wind and solar power systems indicate that

both of the strongly fluctuating renewable power sources are characterized by a power-law PSD with the Kolmogorov exponent $-5/3$; see Ref. 32. The DVI thus helps in identifying the sub-grids in a power grid network that are most susceptible to resonant drivings from a renewable power input or consumer demand fluctuations. A characteristic PSD allows for estimating Fourier components' amplitudes through the relation $\varepsilon(\omega) \propto S(\omega)^{\frac{1}{2}}$. We thus define the DVI for the node i given a noisy perturbation with the PSD $S(\omega)$ driving node k as

$$\begin{aligned} \mathrm{DVI}_i^{(k)} &:= \int_{I_{\mathrm{res}}} S(\omega)^{\frac{1}{2}} \left| \sum_{\ell=0}^{N-1} \frac{\imath\omega v_k^{[\ell]} v_i^{[\ell]}}{-\omega^2 + \imath\alpha\omega + \lambda^{[\ell]}} \right| d\omega \\ &\propto \int_{I_{\mathrm{res}}} \left| \dot{\Theta}_i^{(k)}(\omega, t) \right| d\omega. \end{aligned} \tag{6}$$

Essentially, the DVI is an integral of the (time-independent) response strength $\left|\dot{\Theta}_i^{(k)}(\omega, t)\right|$ for the driving frequency ω over signal's all Fourier components ω in the resonance regime $I_{\mathrm{res}} \subset \mathbb{R}$. The all-time maximum of a node's resonant response magnitude in a time interval of length T is always no larger than the integral of the response strength $\left|\dot{\Theta}_i^{(k)}(\omega, t)\right|$ for the frequency ω over I_{res}, i.e.,

$$\max_{t\in[0,T]} \left| \int_{I_{\mathrm{res}}} \dot{\Theta}_i^{(k)}(\omega, t) d\omega \right| \le \int_{I_{\mathrm{res}}} \left| \dot{\Theta}_i^{(k)}(\omega, t) \right| d\omega. \tag{7}$$

The idea of the DVI is based on the assumption that a node's all-time maximal response[33] [lhs of Eq. (7)] approaches the integral of the resonant response strength [rhs of Eq. (7)] for a sufficiently long time T, which we will examine numerically below. The integral in the definition of DVI [Eq. (6)] can be easily computed in a numerical way so that the relative value of DVI reduces to a discrete sum over Fourier frequency components ω in I_{res}.

Note that the PSD $S(\omega)$ gives only the scaling information of $\varepsilon(\omega)$; therefore, the relative value of DVI among all nodes within a network seems more relevant than its absolute value. The ranking of DVI thus provides information about which nodes are most susceptible rather than predicting the actual response magnitudes. Evaluations of direct numerical simulations show that the DVI ranking is capable of predicting those dynamically vulnerable nodes that are unexpected by intuition or naïve inferences. For instance, in a 100 s simulation (Fig. 2), the ranking of the numerically determined all-time maximal frequency response appears to be highly similar to the ranking given by DVI. Remarkably, it gives warnings that some

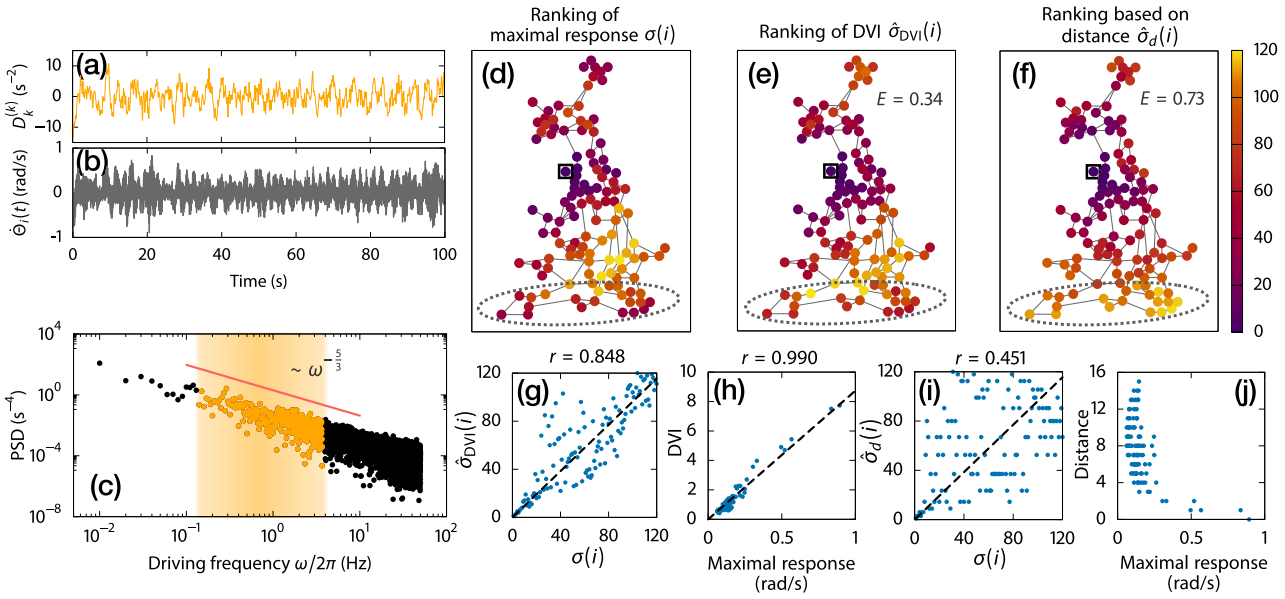

FIG. 2. The ranking of DVI well predicts the ranking of maximal resonant responses. (a) and (b) The grid frequency responses of the British high-voltage power grid to a resonant driving signal with (c) PSD of the Kolmogorov exponent $-5/3$. (c) The signal is extracted from a colored noise by filtering the frequencies (black dots) and keeping only the ones (orange dots) in the resonance regime (shaded in orange). (d) The color-coded actual ranking $\sigma(i)$ of the maximal frequency response $\max_{t\in[0,T]} \left|\dot{\Theta}_i^{(k)}(t)\right|$ in the simulation of $T = 100$ s. (e) and (f) Two predicted rankings: (e) $\hat{\sigma}_{\mathrm{DVI}(i)}$ given by DVI (6) and (f) $\hat{\sigma}_d(i)$ by a (graph-theoretic) distance-based measure, respectively. The ranking $\hat{\sigma}_d(i)$ is tied since multiple nodes share the same graph-theoretic distance and thus is computed using a method by Fagin *et al.*[34] A black square marks the perturbed node, and dotted circles highlight the vulnerable nodes, which are well predicted by DVI but missed by the distance-based measure. The respective prediction error E defined in Eq. (8) is also shown. (g)–(j) The correlation between the true ranking and the two predicted rankings (g) and (i) and the correlation between the value of the maximal responses and the two vulnerability measures (h) and (j). A linear fit (through the origin) and the corresponding Pearson's correlation coefficient r is shown in (g)–(i), while the correlation in (j) is clearly nonlinear. Except the topology, the network settings are the same as in Fig. 1.

particular nodes (e.g., the ones marked in dotted circles) would be especially vulnerable to resonant perturbations. Those nodes would be missed by prediction approaches based solely on topology, such as those assuming that nodes at a smaller graph-theoretic distance to the fluctuation are more strongly effected [compare Figs. 2(d)–2(f)]. Particularly, in power systems frequency regulation devices such as power system stabilizers (PSSs) may extenuate frequency fluctuations in a frequency range I_{PSS} that (partially) overlaps with the resonance frequency range I_{res}. In such settings where some frequencies are missing or strongly reduced in amplitudes, DVI still works in principle because it relies on those frequencies ω present that are largest in amplitudes. Based on theoretical considerations, to the first approximation, the contributions of the respective frequency components should then be excluded in the computation of DVI; i.e., the integration in Eq. (6) should be performed over the interval $I_{\mathrm{res}} \setminus I_{\mathrm{PSS}}$ instead of I_{res}. Numerical simulations confirmed that the adapted DVI still provides good estimates for vulnerable nodes in the presence of frequency regulation mechanisms; these results are qualitatively the same as those presented in Fig. 2 and thus not shown here. Under the same network settings and driving signals as in Fig. 2, the prediction error for estimating the all-time maximum of the regulated response, with frequency components in $I_{\mathrm{PSS}} = (0.1\,\mathrm{Hz}, 1\,\mathrm{Hz})$ filtered out, is 0.33, close to the error 0.34 without any frequency regulation [Fig. 2(e)]. The Pearson correlation coefficient 0.850 between the DVI ranking and the true ranking and the correlation 0.994 between the DVI value and the true maximal response value are qualitatively the same (and even higher) than the values displayed in Figs. 2(g) and 2(h).

We further quantitatively investigate the prediction performance of DVI in terms of its robustness over time and over the stochastic feature of the fluctuation. We measure DVI's prediction error with a normalized Spearman's footrule distance[35] between the predicted ranking $\hat{\sigma}_{\mathrm{DVI}}(i)$ and the actual ranking $\sigma(i)$,

$$E := \frac{1}{E_{\mathrm{rand}}} \sum_{i=1}^{N} \left| \hat{\sigma}_{\mathrm{DVI}}(i) - \sigma(i) \right|. \tag{8}$$

The Spearman's footrule distance measures the disagreement of two rankings of N elements, σ_1 and σ_2, by taking the sum of the absolute values of the difference between them $\sum_{i=1}^{N} |\sigma_1(i) - \sigma_2(i)|$. The prediction error E here is further normalized by the expectation value of the Spearman's footrule distance $E_{\mathrm{rand}} = N^2/3$ between two random rankings chosen independently and uniformly in the set S_N of permutations of N elements; see Ref. 35. Numerical results show that the ranking σ of the maximum response from direct simulation converges fast to the *a priori* DVI ranking $\hat{\sigma}_{\mathrm{DVI}}$ [Fig. 3(a)]. For a 100 s perturbation time series, we measure the true ranking σ every 0.1 s and compute the footrule distance E. For a sample power grid with the eigenfrequencies around 1 Hz ($I_{\mathrm{res}} = [0.32\,\mathrm{Hz}, 3.74\,\mathrm{Hz}]$), the prediction error drops about 80% in the first 10 s and continues to decrease slowly. At $T = 100$ s, the prediction error drops to about 15% of the random guess error level and far below ($< 40\%$) the error of the predictions based on the graph-theoretic distance. The DVI is highly correlated to the maximal frequency responses with Pearson's correlation coefficient r larger than 0.985 [Figs. 3(c)–3(e)]. Furthermore, we find the prediction performance of DVI to be quite robust over time and for different types of colored noise with the power-law exponent $b \in [0, 2]$, from white noise to brown noise. The prediction error remains at almost the same level and shows only a mild increase with growing b [Fig. 3(b)].

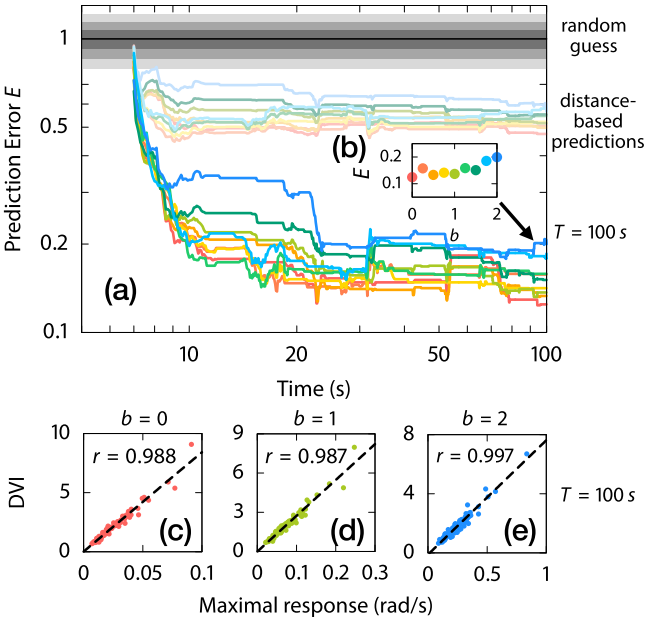

FIG. 3. Fast-converging, robustly high prediction performance of DVI ranking. (a) The prediction error of DVI drops sharply at first, decreases over time, and rests at a level about 85% lower than the error of random guesses. The Gaussian error distribution of random guesses[35] is indicated by various shades of gray: the black line for the expectation value of E for random guesses, areas colored with different shades of gray for intervals $1 \pm \rho$, $1 \pm 2\rho$, and $1 \pm 3\rho$, respectively, with ρ being the ratio between the standard deviation and the expectation value of E for random guesses. The lines with a lower saturation of color indicate a much higher prediction error for the distance-based measure. (b) A snapshot of the prediction error's dependence on signal's PSD exponent b at the end of the simulation $T = 100$ s. The prediction error increases slightly for larger PSD exponents of the driving signal. (c)–(e) At $T = 100$ s, the DVI exhibits a high correlation with the maximal frequency response for the wide range of tested PSD exponents $b \in \{0, 1, 2\}$. In (a)–(e), the lines and disks are color-coded by the signal's PSD exponent b; see (b) for a correspondence. The network settings are the same as in Fig. 1.

IV. CONCLUSION

We presented a measure of dynamic node vulnerability (DVI) to predict the most resonant nodes in stochastically driven oscillator networks and, specifically, AC power grid models. Based on a linear response theory of the network's resonance patterns for a single frequency, we propose to estimate the susceptibility of a node to stochastic driving signals by (i) estimating the driving signal's Fourier spectrum by its PSD characteristics and (ii) accumulating the nodal response amplitudes to each Fourier components. Numerical results indicate strong prediction power of the proposed DVI in identifying the most resonant nodes. The true ranking of a maximum response from direct simulation converges fast to the ranking prediction given by DVI, thus revealing the most vulnerable nodes.

The prediction performance is robust not only over time, but also for various types of colored noise sources. For all tested settings, ranging from white noise to brown noise with a PSD exponent $b \in [0, 2]$, the prediction error stays at a low level, and the DVI highly correlates with the true response, with a Pearson's correlation coefficient larger than 0.985. The proposed DVI largely outperforms an intuitive measure based on the graph-theoretic distance with less than half of the prediction error.

Given the position and the characteristic PSD of the driving signal, for instance, the location of a wind farm in a power grid network, the ranking of the DVI obtained from Eq. (6) may help in identifying which stations in the power grid would particularly be influenced by the resonant signals carried by the fluctuating wind power input, allowing precautionary measures to be taken (see Fig. 2 for an example of the British grid topology). The DVI is also adaptable to power systems with frequency regulation mechanisms providing accurate estimates of dynamically vulnerable nodes. As the method is robust and computationally fast, it might also be applicable *ad hoc* if the network changes after failures or other unforeseen events such as load shedding.

Furthermore, the DVI may support optimizing future power grid planning. For instance, new stations or new lines should be built in a way that important units in the network would not suffer from severe resonant disturbances in the altered network topology.

Taken together, the proposed dynamic vulnerability index provides a powerful tool to rank the nodal resonance level in networks of dynamical units. Whereas the presentation above is focused on the second-order Kuramoto model to overcome previous analytic limitations, the index is readily generalized, both to phase oscillator networks (with single variable nodes) and more complex systems such as networks of the third order model of power grids and more generally, networks of oscillatory and non-oscillatory dynamic units.

ACKNOWLEDGMENTS

We gratefully acknowledge support from the Deutsche Forschungsgemeinschaft (DFG; German Research Foundation) under Germany's Excellence Strategy—No. EXC-2068-390729961—Cluster of Excellence Physics of Life and the Cluster of Excellence Center for Advancing Electronics at TU Dresden, and the German Federal Ministry for Research and Education (BMBF Grant Nos. 03SF0472F and 03EK3055F).

DATA AVAILABILITY

The data that support the findings of this study are available from the corresponding author upon reasonable request.

REFERENCES

[1]F. Hussain, C. Gupta, A. J. Hirning, W. Ott, K. S. Matthews, K. Josic, and M. R. Bennett, "Engineered temperature compensation in a synthetic genetic clock," Proc. Natl. Acad. Sci. U.S.A. **111**, 972–977 (2014).
[2]S. Jahnke, R.-M. Memmesheimer, and M. Timme, "Oscillation-induced signal transmission and gating in neural circuits," PLoS Comput. Biol. **10**, e1003940 (2014).
[3]P. Kundur, N. J. Balu, and M. G. Lauby, *Power System Stability and Control*, The EPRI Power System Engineering Series Vol. 7 (McGraw-Hill, New York, 1994).
[4]G. Filatrella, A. H. Nielsen, and N. F. Pedersen, "Analysis of a power grid using a Kuramoto-like model," Eur. Phys. J. B **61**, 485–491 (2008).
[5]M. Rohden, A. Sorge, M. Timme, and D. Witthaut, "Self-organized synchronization in decentralized power grids," Phys. Rev. Lett. **109**, 064101 (2012).
[6]A. E. Motter, S. A. Myers, M. Anghel, and T. Nishikawa, "Spontaneous synchrony in power-grid networks," Nat. Phys. **9**, 191 (2013).
[7]F. Dörfler, M. Chertkov, and F. Bullo, "Synchronization in complex oscillator networks and smart grids," Proc. Natl. Acad. Sci. U.S.A. **110**, 2005–2010 (2013).
[8]T. Coletta and P. Jacquod, "Linear stability and the Braess paradox in coupled-oscillator networks and electric power grids," Phys. Rev. E **93**, 032222 (2016).
[9]D. H. Zanette, "Propagation of small perturbations in synchronized oscillator networks," Europhys. Lett. **68**, 356–362 (2004).
[10]D. H. Zanette, "Disturbing synchronization: Propagation of perturbations in networks of coupled oscillators," Eur. Phys. J. B **43**, 97–108 (2005).
[11]M. Tyloo, T. Coletta, and P. Jacquod, "Robustness of synchrony in complex networks and generalized Kirchhoff indices," Phys. Rev. Lett. **120**, 084101 (2018).
[12]X. Zhang, S. Hallerberg, M. Matthiae, D. Witthaut, and M. Timme, "Fluctuation-induced distributed resonances in oscillatory networks," Sci. Adv. **5**, eaav1027 (2019).
[13]H. Haehne, K. Schmietendorf, S. Tamrakar, J. Peinke, and S. Kettemann, "Propagation of wind-power-induced fluctuations in power grids," Phys. Rev. E **99**, 050301 (2019).
[14]B. Schäfer, M. Matthiae, X. Zhang, M. Rohden, M. Timme, and D. Witthaut, "Escape routes, weak links, and desynchronization in fluctuation-driven networks," Phys. Rev. E **95**, 060203 (2017).
[15]S. Kettemann, "Delocalization of disturbances and the stability of ac electricity grids," Phys. Rev. E **94**, 062311 (2016).
[16]S. Tamrakar, M. Conrath, and S. Kettemann, "Propagation of disturbances in ac electricity grids," Sci. Rep. **8**, 6459 (2018).
[17]D. Manik, M. Rohden, H. Ronellenfitsch, X. Zhang, S. Hallerberg, D. Witthaut, and M. Timme, "Network susceptibilities: Theory and applications," Phys. Rev. E **95**, 012319 (2017).
[18]B. Schäfer, C. Beck, K. Aihara, D. Witthaut, and M. Timme, "Non-Gaussian power grid frequency fluctuations characterized by Lévy-stable laws and superstatistics," Nat. Energy **3**, 119 (2018).
[19]M. Tyloo, R. Delabays, and P. Jacquod, "Noise-induced desynchronization and stochastic escape from equilibrium in complex networks," Phys. Rev. E **99**, 062213 (2019).
[20]J. Hindes, P. Jacquod, and I. B. Schwartz, "Network desynchronization by non-Gaussian fluctuations," arXiv:1904.12174 (2019).
[21]M. Tyloo, L. Pagnier, and P. Jacquod, "The key player problem in complex oscillator networks and electric power grids: Resistance centralities identify local vulnerabilities," arXiv:1810.09694 (2018).
[22]S. Auer, F. Hellmann, M. Krause, and J. Kurths, "Stability of synchrony against local intermittent fluctuations in tree-like power grids," Chaos **27**, 127003 (2017).
[23]A. Plietzsch, S. Auer, J. Kurths, and F. Hellmann, "A generalized linear response theory of complex networks with an application to renewable fluctuations in microgrids," arXiv:1903.09585 (2019).
[24]S. Arianos, E. Bompard, A. Carbone, and F. Xue, "Power grid vulnerability: A complex network approach," Chaos **19**, 013119 (2009).
[25]I. Simonsen, L. Buzna, K. Peters, S. Bornholdt, and D. Helbing, "Transient dynamics increasing network vulnerability to cascading failures," Phys. Rev. Lett. **100**, 218701 (2008).
[26]R. Albert, I. Albert, and G. L. Nakarado, "Structural vulnerability of the North American power grid," Phys. Rev. E **69**, 025103 (2004).
[27]H. Song and M. Kezunovic, "Static security analysis based on vulnerability index (VI) and network contribution factor (NCF) method," in *2005 IEEE/PES Transmission & Distribution Conference & Exposition: Asia and Pacific* (IEEE, 2005), pp. 1–7.
[28]G. Qu, J. Rudraraju, R. Modukuri, S. Hariri, and C. S. Raghavendra, "A framework for network vulnerability analysis," in *IASTED International Conference on Communications, Internet, and Information Technology, St. Thomas, US Virgin Islands, 18–20 November 2002* (ACTA Press, 2002), pp. 289–294.
[29]R. Gutiérrez, F. Del-Pozo, and S. Boccaletti, "Node vulnerability under finite perturbations in complex networks," PLoS One **6**, e20236 (2011).

[30]M. Tyloo and P. Jacquod, "Global robustness vs. local vulnerabilities in complex synchronous networks," arXiv:1905.03582 (2019).
[31]P. Schultz, J. Heitzig, and J. Kurths, "A random growth model for power grids and other spatially embedded infrastructure networks," Eur. Phys. J. Spec. Top. **223**, 2593–2610 (2014).
[32]M. Anvari, G. Lohmann, M. Wächter, P. Milan, E. Lorenz, D. Heinemann, M. R. R. Tabar, and J. Peinke, "Short term fluctuations of wind and solar power systems," New J. Phys. **18**, 063027 (2016).
[33]Here, the response, as a physical quantity, refers to the real part of the complex extension of $\dot{\Theta}_i^{(k)}(t)$.
[34]R. Fagin, R. Kumar, M. Mahdian, D. Sivakumar, and E. Vee, "Comparing and aggregating rankings with ties," in *Proceedings of the Twenty-Third ACM SIGMOD-SIGACT-SIGART Symposium on Principles of Database Systems* (ACM, 2004), pp. 47–58.
[35]P. Diaconis and R. L. Graham, "Spearman's footrule as a measure of disarray," J. R. Stat. Soc. Ser. B **39**, 262–268 (1977).